Geospace Magnetic Storms and the Van Allen Radiation Belts

Geoffrey D. Reeves and Ioannis A. Daglis

3.1 Introduction	52
3.2 Electron motion in Earth's radiation belts	53
3.3 Effects of geospace magnetic storms on the radiation belts	55
3.4 Local acceleration and radial diffusion	61
3.5 Phase space density gradients	66
3.6 Studies with the Van Allen Probes: insights into the effects of wave-particle interactions and the ring	
current influence	69
3.7 Summary	72
Acknowledgments	72
References	73

■ Abstract

The dynamics of geospace magnetic storms and changes in the Van Allen radiation belts are intimately intertwined. At the simplest level, the build-up and decay of the storm-time ring current and of the radiation belts are fundamentally similar: electrons and ions are injected into the inner magnetosphere, where they are further accelerated to form the ring current and radiation belts. Both populations decay gradually, after elevated magnetospheric activity has ceased. The ring current decays primarily by charge exchange and the radiation belts decay primarily by atmospheric precipitation. Digging even slightly deeper than this simplistic description, however, uncovers many unanswered questions, which are addressed in this chapter.

3.1 Introduction

The two major charged particle populations that are trapped by the geomagnetic field in geospace are the Van Allen radiation belts and the ring current. They are distinguished by their high energies (~10 to 500 keV for the ring current, ~100 keV to 20 MeV / 200 MeV for the radiation belt electrons/protons), when compared to much lower energies of the surrounding plasmas, and by their intricate relationship during the most complex phenomenon of solar-terrestrial coupling—the geospace magnetic storms. The lower energy end of these populations—the ring current—is the main cause of the defining feature of magnetic storms: the worldwide reduction of the geomagnetic field horizontal component, which is evident in the storm-time Dst index profile. The higher energy end of these populations—the radiation belts—was the first component of magnetospheric plasma, and space plasma in general, to be discovered at the very beginning of the space era.

The milestone discovery of the radiation belts was made through the measurements of Geiger-Müeller tubes of the group of Professor James Van Allen on board the Explorer 1 and 3 satellites in 1958 [Van Allen et al., 1958]. Van Allen correctly interpreted those measurements as a result of intense corpuscular radiation [Van Allen, 1959]. The first source proposed for the origin of the radiation belts was decay of neutrons produced by the interaction of cosmic rays with the Earth's atmosphere [Singer, 1958; Kellogg, 1959; Vernov et al., 1959]. Balloon and rocket measurements, however, showed that the loss rates of radiation belt electrons through precipitation into the atmosphere [e.g., Winckler et al., 1962] would have demanded improbably high rates of replenishment if cosmic rays had been the source. The time dependence of outer belt electron fluxes was even more problematic [see, e.g., Walt, 1996], but, until spectral measurements became available, variations in detector count rates could potentially be explained by more subtle changes in spectral slope—an ambiguity that would resurface, for different reasons, in the observations from the 1990s and 2000s. In contrast, the proposal by Kellogg [1959] that neutron albedo might be responsible for protons in the radiation belts is now widely accepted [e.g., Selesnick et al., 2007]. To this date, we generally think of the Earth's radiation belts as consisting of two belts of energetic particles—a very stable inner belt in the region $L < \sim 2$ composed of both energetic electrons and ions and a very dynamic outer belt in the region $L > \sim 3$ that is composed almost entirely of electrons. However, recent results have shown that multiple belt structures exist [Baker et al., 2013] and that the nature of the slot and the inner belt-even their existence-is highly energy-dependent [Fennell et al., 2015; Reeves, 2015]. The region of relatively lower radiation levels in the region L \approx 2–3 is referred to as the slot region. In this chapter we focus primarily on the dynamic outer belt electron population.

The other major energetic particle population in geospace is the ring current—the electric current responsible for the global depression of the magnetic field's horizontal component on Earth's surface. Although the ring current is carried by both electrons and ions, most of its energy density is due to medium-energy (tens of keV) ions [e.g., Williams, 1981; Daglis et al., 1993]. The existence of a giant diamagnetic

ring current encircling Earth had been predicted long before its actual observation in space [e.g., Chapman and Ferraro, 1930, 1931]. Early OGO-3 satellite measurements in the 1960s analysed by Frank [1967] confirmed the existence of the ring current and showed that the ring current is dominated by ions with energies around 50 keV. The detailed composition and energy of the ring current were not clarified until the Active Magnetospheric Particle Tracer Explorer (AMPTE) mission of the late 1980s [e.g., Hamilton et al., 1988; Daglis et al., 1993]. A few years later, the Combined Release and Radiation Effects Satellite (CRRES) confirmed and expanded the conclusions of the AMPTE mission, especially with regard to intense magnetic storms [e.g., Daglis, 1997].

The dynamics of geospace magnetic storms and of the ring current and changes in the Earth's radiation belts are intimately intertwined. At the most simple level the build-up and decay of both the ring current and radiation belts are fundamentally similar: electrons and ions are injected into the inner magnetosphere where they are further accelerated to form the ring current and radiation belts. Both gradually decay after activity has stopped. The ring current decays primarily by charge exchange and the radiation belts decay primarily by atmospheric precipitation. Digging even slightly deeper than this simplistic description, however, uncovers many unanswered questions. How do injected electrons and ions get trapped in the inner magnetosphere? What processes accelerate these 'seed' populations? What controls the structure and the evolution of the ring current and radiation belts? Where are they most intense and why does that vary from event to event? How are the overall intensities of the ring current and radiation belts related? How do ring current processes affect the radiation belts? Those questions, and their implications for space weather, were among the primary motivations for the NASA Van Allen Probes mission, launched in August 2012 [Mauk et al., 2012].

In this chapter we will attempt to provide a few representative examples of the developments that have led to our current understanding as well as examples that point to some of the holes in our understanding [following the treatment in Reeves, 2015]. Although the radiation belts may play some role in controlling ring current dynamics, the dominant coupling is in the opposite direction. Therefore we will primarily focus on aspects of ring current dynamics that have important effects on the radiation belts. The most prominent effects are those of various ring current driven electromagnetic waves on radiation belt electrons [e.g., Bortnik et al., 2006; Ozeke and Mann, 2008]. We also emphasize that this paper does not provide a review of recent results from the ongoing Van Allen Probes mission but direct the interested reader to http://rbspgway.jhuapl.edu/biblio for a current bibliography.

3.2 Electron motion in Earth's radiation belts

Very quickly after the discovery of the radiation belts, Northrop and Teller [1960] had worked out the equations of motion that govern adiabatic motion in the geomagnetic field

and derived the invariants associated with electron gyromotion (μ) , bounce between mirror points (J or K), and drift azimuthally around the Earth (Φ or L*). These invariants are approximately conserved under slow changes to the magnetic field, fully describe relativistic electron motion in an arbitrary geomagnetic field configuration, and are fundamental to understanding the dynamics of the radiation belts and their coupling to the ring current.

The first invariant, μ , is associated with the electron gyro-motion around the magnetic field and is given by

$$\mu = \frac{p_{\perp}^2}{2m_0 B}$$

where m_0 is the rest mass, and p_{\perp} is the relativistic momentum in the direction perpendicular to the magnetic field, B.

The second invariant is associated with the bounce motion between the Northern and Southern mirror points:

$$\mathcal{J}=\oint p_{\parallel}ds=2\int_{s_{R}}^{s_{S}}p_{\parallel}ds.$$

When μ is conserved, the second invariant can also be expressed in a convenient form that is independent of energy

$$K = \frac{\mathcal{F}}{2\sqrt{2m_0\mu}} = \int_{s_c}^{s_n} \sqrt{B_m - B(s)} \, ds$$

where B_m is the magnetic field strength at the mirror point and s is the path length along the field line. The third invariant is an integral around the drift path and between the mirror points:

$$\Phi = \oint \vec{B} \bullet d\vec{A}$$

which conserves the total magnetic flux enclosed within a drift shell. In radiation belt physics it is more common to use the L* parameter [Roederer, 1970]

$$L^* = \frac{2\pi M}{\Phi R_E}$$

where M is the Earth's magnetic moment and R_E is the radius of the Earth (6,371 km). In a dipole magnetic field $L^* = L$ (sometimes called 'McIlwain L'). However, when the field is not a pure dipole L^* is not equivalent to L. In a realistic field, electrons



Figure 3.1 A visualization of radiation belt drift shells based on numerical particle tracing in a realistic geomagnetic field [Reeves et al., 2012]. Mirror points for different equatorial pitch angles (in 10° steps) are shown spaced along the field. As electrons drift around the Earth, conservation of μ and K requires that the electrons follow different drift paths as indicated by the colour-coded field lines. Drift shell splitting is particularly apparent in the upper right of the figure. Electrons measured at the satellite, with 30° pitch angles, move along the copper-coloured surface which is the drift shell for those electrons. On that drift shell, μ , K, and L^* are constant but pitch angle, energy, and radial distance are not.

with different pitch angles follow different drift paths—an effect known as drift shell splitting (Figure 3.1). Therefore, electrons with different pitch angles, measured at a given point in space (such as a specific satellite location), have different third invariants, Φ , and therefore different L*. That means that, while a given point in space can have a single value of L for all electrons on the field line, it cannot be assigned a single value of L*.

3.3 Effects of geospace magnetic storms on the radiation belts

One of the primary drivers of change and spatial asymmetry in the Earth's magnetic field (particularly deep in the inner magnetosphere) is the storm-time ring current [Daglis et al., 1999; Daglis, 2006]. The ring current dramatically modifies the geomagnetic field and thus 'causes' geospace magnetic storms. Strong geomagnetic field variations

influence, in turn, dramatically the properties of radiation belt electrons, because they affect all three periodic motions of electrons.

Conservation of the first adiabatic invariant implies that changes in the local magnetic field magnitude must also produce changes in the perpendicular momentum, which changes the electrons' energy and pitch angle and therefore their magnetic mirror points.

Magnetic storms typically involve intense stretching and subsequent dipolarization of the night-side magnetic field. Since the second invariant is an integral along the field between the mirror points, conservation of J will also redistribute radiation belt electrons in a strongly pitch-angle dependent way. Stretching of the night-side field increases drift shell splitting, moving equatorially mirroring electrons closer to Earth on the night-side and field-aligned electrons away from the Earth. Combined with the typical radial gradients, the stretching of the field produces a change in the local pitch angles toward a 'butterfly' distribution with a minimum at 90°. At the same time a satellite can find itself on field lines that now map much further down the tail and toward the outer boundary of the radiation belts.

The third invariant Φ or L* is an integral of the magnetic flux enclosed in a drift path. An increase in the storm-time ring current decreases the magnetic field strength in the inner magnetosphere and electrons must move outward in order for their drift orbits to enclose the same flux – an effect known as the 'Dst effect' [Kim and Chan, 1997] (Figure 3.2). This outward motion moves electrons to even lower local field magnitudes, further reducing their energy. Measured at a fixed energy, this appears as a reduction (or dropout) of fluxes.

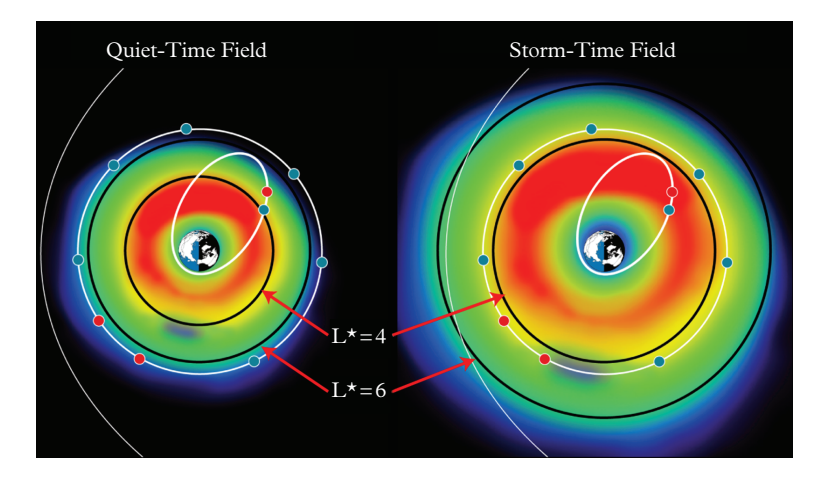


Figure 3.2 A schematic visualization of the Dst effect [Reeves et al., 2012]. As the ring current intensifies and the magnetic field strength in the inner magnetosphere decreases, radiation belt electrons move outward to conserve the third adiabatic invariant. Fluxes (in colour) are arbitrary and L-shells are not shown quantitatively.

On storm time scales (hours to days), changes in the geomagnetic field change motion of radiation belt electrons adiabatically. In other words there is no net, permanent effect on the electrons due to changes in the field alone and when the field returns to its pre-storm state the radiation belt electrons will too. Therefore any other changes in the radiation belts have to be understood in the context of those adiabatic changes. To understand radiation belt processes, one must disentangle both adiabatic and non-adiabatic storm-time processes that, typically, occur simultaneously.

For example, as shown in Figure 3.2, some drift paths (constant L*) moving adiabatically outward encounter the magnetopause and electrons on those drift shells are permanently lost from the radiation belts. When the field will relax to its pre-storm configuration those drift shells will exhibit a net (non-adiabatic) loss of electrons, while other drift shells will exhibit only a temporary (adiabatic) decrease in fluxes with no net loss. Other non-adiabatic storm-time processes that affect the radiation belt include intensification of ULF waves that enhance radial diffusion of radiation belt electrons, injection of intensified population of substorm-accelerated electrons that can form a seed population for further acceleration to relativistic energies, formation of unstable plasma distributions producing VLF waves that resonantly interact with radiation belt electrons, and changes in ion composition that can also affect plasma instabilities and field-line resonant frequencies.

All of the processes affecting radiation belt electrons (both adiabatically and non-adiabatically) are typically enhanced during magnetic storms. Therefore it was natural to assume that intense magnetic storms would produce big radiation belt enhancement events. Reeves [1998] attempted to demonstrate this relationship, but found instead that, while most radiation belt enhancements (at geosynchronous orbit) occur during storms, the intensity of radiation belt enhancements is not correlated with the intensity of the storm-time ring current (Figure 3.3).

Shortly thereafter Onsager et al. [2002] showed that magnetic storms do not just enhance the radiation belts—they can also produce non-adiabatic, permanent loss (or dropout) of electrons from the radiation belts. Additionally, they demonstrated that the dropouts typically showed an admixture of adiabatic and non-adiabatic processes that produced different responses at different times.

In a follow-on study Reeves et al. [2003] surveyed 276 moderate and intense storms (min Dst < -50 nT) from 1989 through 2000, showing examples of storms that intensified the radiation belts, storms that depleted the radiation belts, and storms that produced no net change in the radiation belts (Figure 3.4). They also compared statistically the maximum fluxes at geosynchronous orbit 1–3 days before the storm with the maximum flux 1–5 days after the storm and found that 53% of storms increased, 19% decreased, and 28% had no net effect on the intensity of the radiation belt fluxes.

Many studies have focused on the radiation belt response during storms but few studies have looked systematically at the ring current conditions during radiation belt events. This is in part due to the fact that it is easy to categorize storms by minimum Dst but there is no widely accepted way to quantitatively define a radiation belt event. On the other hand, some recent studies showed that radiation belt enhancements could be observed even in the absence of magnetic storms [Schiller et al., 2014; Su et al., 2014b].

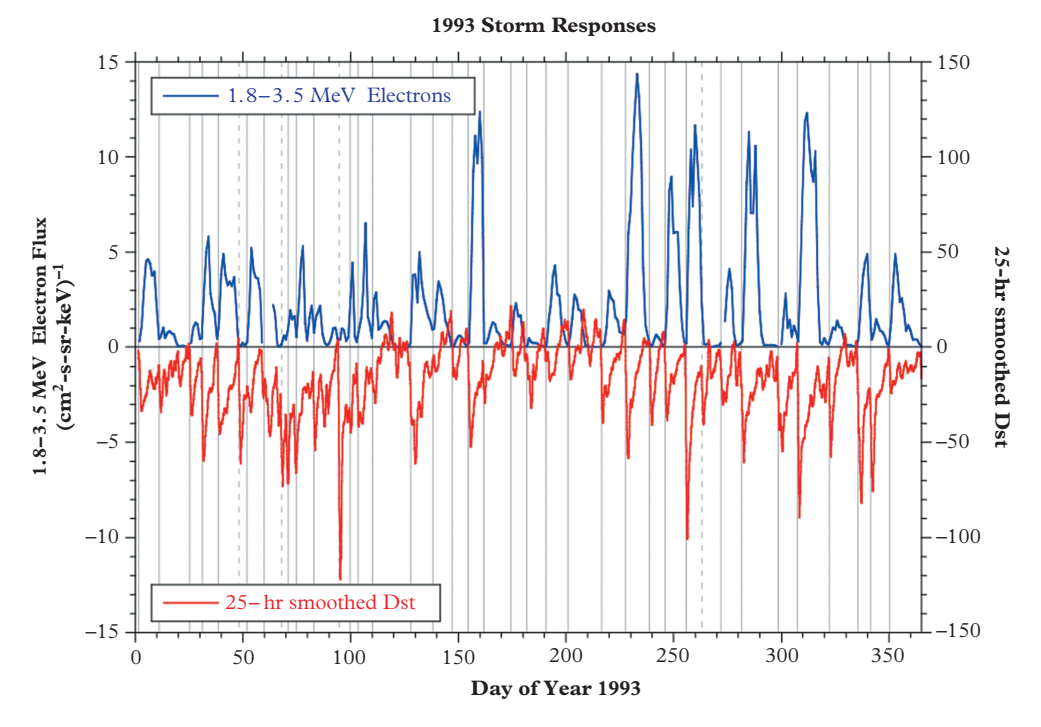
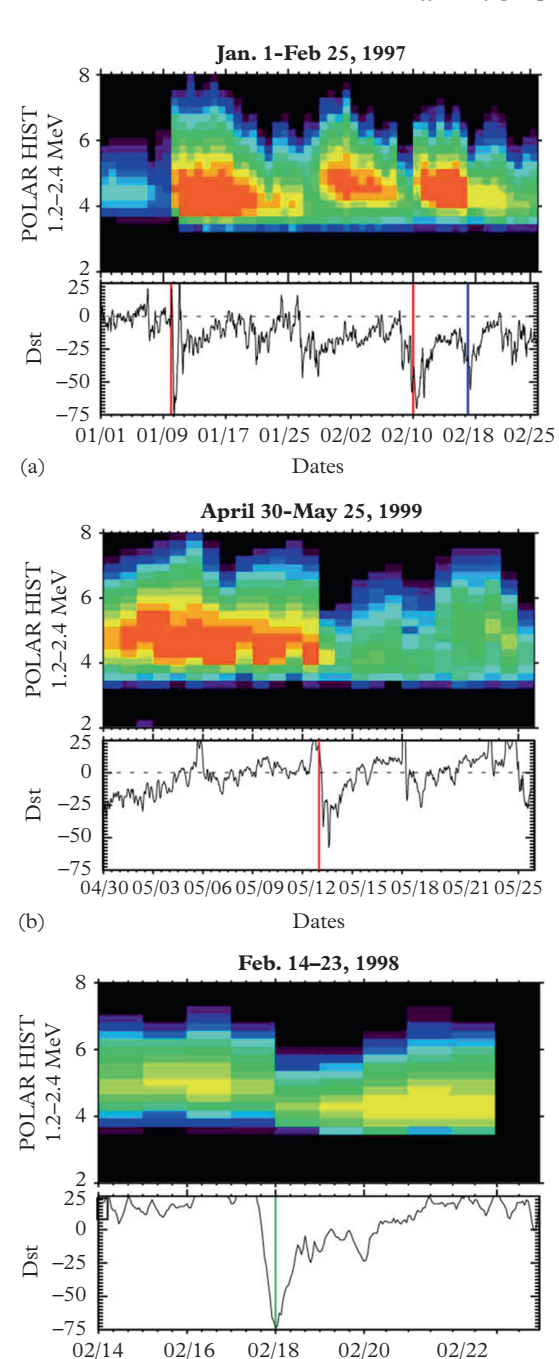


Figure 3.3 Relativistic electron fluxes measured at geosynchronous orbit (blue) and 25-hour smoothed Dst (red) in 1993—a year dominated by recurrent coronal hole high-speed streams. During all phases of the solar cycle, radiation belt electron enhancements typically occur in association with storm-time decreases in Dst but the intensities are not correlated. Strong storms do not necessarily produce strong radiation belt enhancements.

In contrast to the studies discussed earlier, Tverskaya et al. [2003] found a rather consistent and repeatable radiation belt response to storms. They examined the location of the peak of the radiation belts as a function of Dst. Using data from the Polar, HEO, and SAMPEX satellites they confirmed and extended the results of an earlier study [Tverskaya, 1986] showing that the location of peak \sim 2 MeV electron flux could be described by the relationship $|\mathrm{Dst}|_{\mathrm{max}} = 2.75 \times 10^4 \ / \ L_{\mathrm{max}}^4$, independently of the actual flux of radiation belt electrons (Figure 3.5). The reason why this remarkable relationship should exist has not yet been fully explained. Similarly the results of Tverskaya et al. [2003] have not been reconciled with the results of Reeves et al. [2003], who reported that the percentage of storms that increased (or decreased) the intensity of the belts was independent of L-shell (see also Figure 3.5).

Other evidence of the relationship between magnetic storms and the radiation belts came from studies of the seasonal dependence of relativistic electron fluxes [Baker et al., 1999]. Averages performed over three-month intervals, centred on the spring and fall equinoxes and on the winter and summer solstices, showed that equinoctial fluxes of



Dates

(c)

Figure 3.4 Examples of storms that (A) increased radiation belt fluxes, (B) decreased fluxes, and (C) left the belts relatively unchanged (less than a factor of 2 net change in flux) [from Reeves et al., 2003].

©John Wiley and Sons 2003.

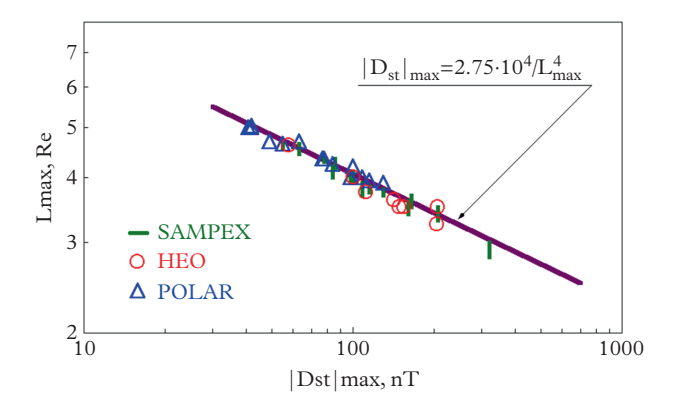


Figure 3.5 Tverskaya et al. [2003] showed a remarkably consistent and repeatable relationship between the location of the peak flux of 2 MeV electrons in the radiation belts (L_{max}) with maximum magnetic storm intensity ($|Dst|_{max}$). Tverskaya et al. [2003]

electrons are nearly a factor of three larger than the solstitial fluxes based upon a superposed epoch analysis for 1992–1999. They concluded that both the radiation belts and the ring current respond similarly to more efficient merging of the interplanetary and the magnetospheric magnetic fields near the equinoxes [Russell and McPherron, 1973].

It has long been known that radiation belt electron fluxes tend to be higher when solar wind velocities are higher [Paulikas and Blake, 1979]. Solar wind speeds tend to be highest in the declining phase of the solar cycle when driving can be dominated by corotating interaction regions (CIRs) produced by high-speed streams (HSS) from solar coronal holes [Blake et al., 1997; Baker et al., 1998; Reeves, 1998]. This relationship led researchers to consider whether specific structures in CIRs were particularly effective in driving magnetospheric processes that accelerate radiation belt electrons, and therefore whether increases and decreases in radiation belt fluxes during storms might be related to the type of solar wind drivers [Miyoshi and Kataoka, 2005; Borovsky and Denton, 2006; Clilverd et al., 2010; Borovsky and Denton, 2011; Denton and Borovsky, 2012; Xiao-Fang et al., 2013; Hietala et al., 2014; Kilpua et al., 2015].

In general, CME-driven storms are more effective than CIR-driven storms in producing a strong enhancement of the ring current—even when the integrated southward IMF is approximately the same—but there can also be other differences. Miyoshi and Kataoka [2005] selected storms with –130 nT < Dst < –100 nT and categorized them as CME-driven or CIR-driven (Figure 3.6). They found that 'CIRs are significantly more effective for the evolution of the outer belt than CMEs' and speculated that this was due to 'the existence of a series of particle injections driven by Alfvén waves within the fast coronal hole stream following the CIR'. Miyoshi and Kataoka also selected a third category—of CME-driven great storms with Dst < –130 nT, which produced no stronger radiation belt response than CME-driven intense storms (–130 nT < Dst

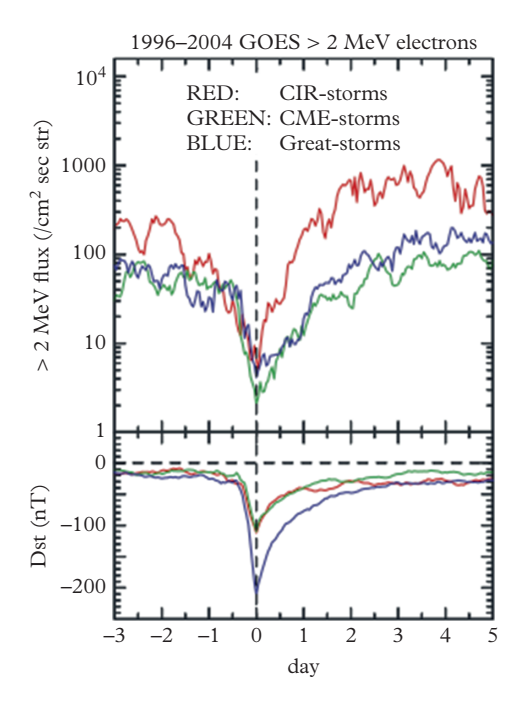


Figure 3.6 Miyoshi and Kataoka [2005] showed that when CIR- and CME-driven storms are selected based on the same minimum Dst, CIR storms 'produce' on average a greater intensification of radiation belt electrons. CME-driven great storms with Dst < -130 nT did not produce any stronger radiation belt response than CME-driven storms with -130 nT < Dst < -100 nT. © John Wiley and Sons 2005.

< -100 nT). On the other hand, it is important to note that only CME-driven great storms (Dst < -130 nT) were effective in enhancing the flux of RB electrons in the inner portion at L < 4 where the slot region exists before the storm onset. This is consistent with previous conclusions that the peak position of the outer belt strongly depends on the Dst index (i.e., the storm intensity) and on the plasmapause position [O'Brien et al., 2003; Miyoshi et al., 2004].

The findings of Miyoshi and Kataoka indicated that storms of different interplanetary causes influence radiation belts differently even when their intensity is comparable. This implied that different storm drivers favour specific storm-associated processes that have distinct impacts on belt dynamics. It became clear that a complete understanding of the relationship between magnetic storms and radiation belt electrons would come from a comprehensive understanding of the various storm-associated processes that have synergetic or competing effects on relativistic electron acceleration and losses [Friedel et al., 2002 and Millan and Thorne, 2007 respectively].

3.4 Local acceleration and radial diffusion

Radiation belt particles are typically measured as particle number flux—a function of spatial position, particle energy, and pitch angle, $j = j(\mathbf{R}, E, alpha)$ —which is not an adiabatically conserved quantity. As discussed previously, in a time-varying geomagnetic

field the flux of radiation belt electrons at a fixed point in space can change dramatically, as electrons adjust their motion to conserve their invariants in the changing magnetic field. Unlike flux, phase space density, $f = j/p^2$, is conserved in a changing magnetic field. Therefore when $j = j(\mathbf{R}, E, \text{alpha})$ is transformed to $f(\mu, K, L^*)$ we can distinguish non-adiabatic electron acceleration, transport, and loss from the 'Dst effect' and other purely adiabatic effects.

Adiabatic motion, by definition, results in no net changes to the electron distribution but Fälthammar [1965] and, later on, other researchers showed that acceleration of radiation belt electrons could occur through radial diffusion when field fluctuations occur on the time scale of electron drifts. He concluded: 'when the first and second invariants are conserved, any radial motion of the particles is associated with a corresponding energy change. Some particles move outward and others inward; but, if there is a source in the outer magnetosphere and a sink farther in, there will be net inward transport and associated net energy gain'. Dungey [1963], on the other hand, proposed that resonant interaction between electromagnetic whistler-mode waves and radiation belt electrons could form a sink for electrons by pitch angle scattering electrons into the atmospheric loss cone. He concluded that 'the effect is found to be important between the inner and outer belts'—the region that is called the slot region near L \approx 2. Lyons and Thorne [1973] showed, quantitatively, that the quiet-time structure of the outer electron belt could be 'explained on the basis of a balance between pitch angle scattering loss and inward radial diffusion from an average outer zone source'. These studies and others, including the comprehensive treatment by Schulz and Lanzerotti [1974], established the fundamental paradigm for radiation belt dynamics: acceleration by inward radial diffusion and loss by pitch angle scattering into the atmosphere.

However, electrons with energies >5 MeV are often enhanced after a storm—even at geosynchronous orbit where the distance to the trapping boundary and, therefore, the amount of energy that can be gained by inward transport from the plasma sheet are small. Energetic electrons in the near-Earth plasma sheet quickly gradient-curvature drift out of the magnetotail so there is never a 'reservoir' of multi-MeV electrons outside the trapping boundary. How then, can we account for the geosynchronous observations? Baker et al. [1989] suggested that the 'recirculation model' developed to explain electron observations at Jupiter [Nishida, 1976] might also apply in the Earth's radiation belts and this modification of the standard radial diffusion paradigm was widely adopted by radiation belt scientists. In the recirculation model (Figure 3.7) electrons radially diffuse inward gaining energy while conserving the first two adiabatic invariants (step 1). In the slot region the pitch angle scattering rates exceed the radial diffusion rates and the particles are scattered toward the atmosphere (step 2). At low altitude the electrons are scattered across field lines without substantial loss of energy (step 3). They are then free to repeat the cycle. While the details were problematic (particularly step 3) the recirculation model had several advantages. It naturally accounted for the 2-3 day build-up of electron fluxes following the commencement of a storm and the very high energies seen at geosynchronous orbit. Recirculation could also explain acceleration up to arbitrarily high energies even at geosynchronous orbit.

Challenges to the recirculation model began to emerge as simultaneous multi-satellite measurements started to become widely available. Energetic particle measurements from

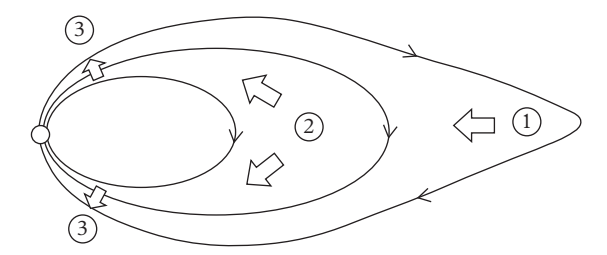


Figure 3.7 A schematic of the 'recirculation' model for radiation belt acceleration [from Nishida, 1976].

GOES and Los Alamos National Laboratory (LANL) instruments at geosynchronous orbit provided near-global coverage, albeit in a narrow range of L-shells. Combining geosynchronous measurements with data from other orbits (SAMPEX, GPS, HEO, and others) started to fill in a three-dimensional picture of the radiation belts [Friedel et al., 1999]. Perhaps even more importantly, multi-satellite studies could overcome the inherent limitation of satellite *orbital periods (typically 12 to > 24 hours)* and provide measurements at multiple L-shells on time scales less than an hour. Multi-satellite analysis made new, detailed studies of space weather events possible. One of the first such studies was a radiation belt enhancement event in November 1993 [Li et al., 1997].

Another such event, in January 1997, was exceptionally well studied [Baker et al., 1998; Goodrich et al., 1998; Jordanova et al., 1998; Kamide et al., 1998; Reeves et al., 1998a; Reeves et al., 1998b; Jordanova et al., 1999; Hudson et al., 2000; Lyons et al., 2000; Hudson et al., 2001]. Following a procedure similar to that used by Li et al. [1997], Reeves et al. [1998a] binned data from 11 satellites in different orbits according to L-shell. Near geosynchronous orbit, L≈6.6, the 2 MeV radiation belt electrons showed their 'typical' behaviour—a gradual build-up of fluxes over ~4 days (with a less typical shock compression early in the event). The behaviour was startlingly different in the heart of the outer radiation belt at L \approx 4.6—where the GPS satellites cross the equatorial plane (Figure 3.8a). There, the 2 MeV electrons shot up by over two orders of magnitude in less than 12 hours. Following the initial acceleration, fluxes remained remarkably constant and showed no evidence of the gradual build-up seen at geosynchronous orbit. In fact, the acceleration was so rapid that the radial profiles seen by GPS satellites moving away from the equator (i.e., outward in L) measured significantly different fluxes than on the inbound part of the orbit even though inbound and outbound measurements at the same L-shell were separated by less than an hour (Figure 3.8b, top). The gradual build-up of fluxes seen near geosynchronous orbit appeared to be the result of outward radial diffusion from the newly accelerated population near L \approx 4.6 (figure 3.8b, top). It is interesting to contrast these high-time resolution measurements with observations from a single satellite. The Polar satellite, with an ~18-hour orbit, captured the state of the belts before and after the acceleration (Figure 3.8b, bottom) but could not resolve the acceleration event itself.

Reeves et al. [1998a] drew two conclusions from the January 1997 event. Firstly, the observations were not consistent with the recirculation model. One of the strengths of the recirculation model was that it naturally explained the gradual build up to a delayed peak that is characteristic of radiation belt observations at geosynchronous orbit. For January

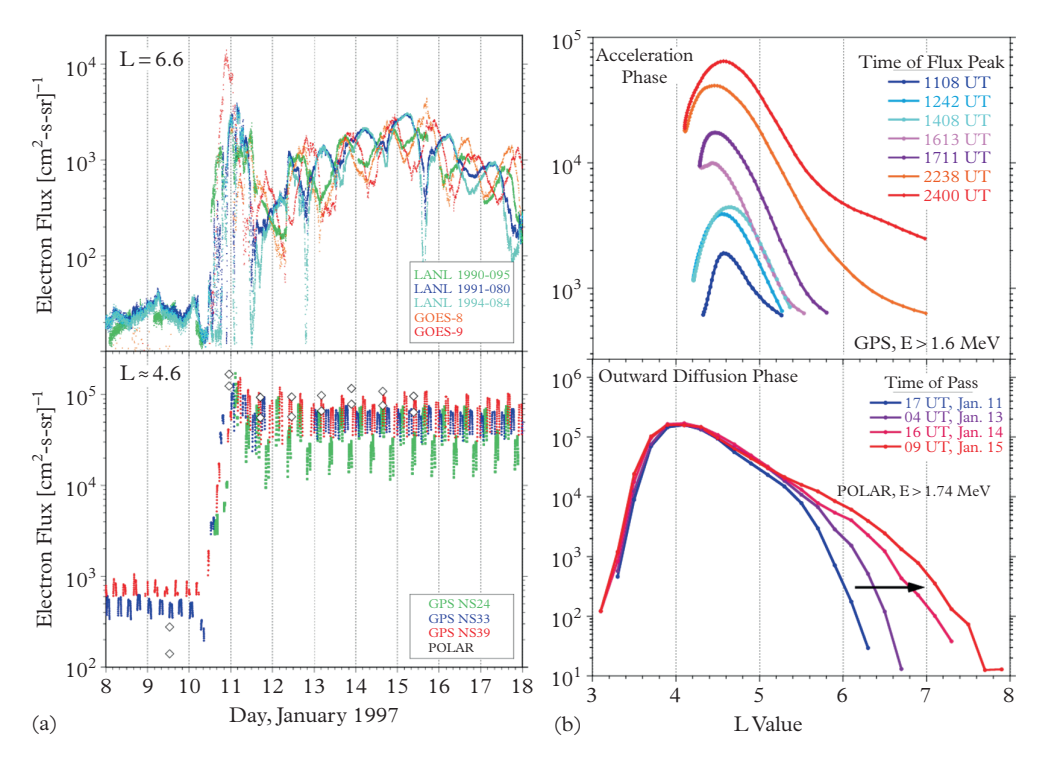


Figure 3.8 Multi-satellite electron observations during the January 1997 radiation belt event [from Reeves et al., 1998a]. Rapid acceleration in the heart of the radiation belts ($L \approx 4.6$) and geosynchronous orbit ($L \approx 6.6$) suggested local acceleration and subsequent outward radial diffusion. But, without phase space density observations, the results were not definitive. © John Wiley and Sons 1998.

1997, the geosynchronous observations still showed that delay. In the recirculation model that delay should be observed at all L-shells as electrons complete the energization loop sketched in Figure 3.7. Instead at $L\approx$ 4.6 the energization was not only much faster but also short-lived, with almost no change in flux after January 12. Secondly, if the electrons were accelerated inside geosynchronous orbit and diffused outward then the acceleration region would have to be confined to a remarkably narrow range of L-shells, well inside geosynchronous orbit, in the heart of the outer belt. If true then the source of the MeV radiation belt electrons would not be the magnetotail, but rather the source would be lower-energy electrons in that same spatial region—somewhere between the plasmasphere and the geosynchronous orbit.

At the same time that new missions and multi-satellite studies were providing a new window on radiation belt dynamics, new theories of relativistic electron acceleration were being developed and included localized acceleration processes deep in the radiation belts. The new studies built on the pioneering work of Dungey [1963] and

Kennel and Petschek [1966], who showed that the VLF whistler-mode waves which pitch-angle scattered electrons into the atmosphere could be produced by plasma distributions with temperature anisotropies unstable to the growth of whistler-mode waves. The (suprathermal) electron temperature anisotropy excites whistler-mode waves, which cause pitch-angle scattering of electrons toward the loss cone. In the late 1990s Summers et al. [1998] proposed that cyclotron resonant interactions at much higher (relativistic) energies have the opposite effect, diffusing electrons toward 90° while simultaneously increasing their energy. At MeV energies, gradients in the energy dimension implied that the flow of energy is from the waves to the particles providing a mechanism for accelerating electrons in situ from the local population of lower-energy electrons.

This 'local acceleration' scenario suggested a more complex and interdependent set of processes might be responsible for acceleration of radiation belt electrons to MeV energies. First electrons must be transported from the magnetotail to the inner magnetosphere by processes such as substorm injections and enhanced large-scale convection—the same processes that produce the storm-time ring current. In the process a fraction of the magnetotail electrons are energized to form a seed population of electrons with energies from a few keV to a few 100s keV. Temperature anisotropies at lower energies (<30 keV) provide a source of free energy for the generation of whistler-mode waves while higher-energy electrons (≈100–500 keV) provide a 'seed' population that can be accelerated to MeV energies by those same waves.

These theories of local acceleration were to undergo further subsequent development [e.g., Horne and Thorne, 1998; Horne et al., 2000; Summers and Ma, 2000; Horne, 2002; Summers et al., 2002; Horne and Thorne, 2003; Summers et al., 2004; Albert and Young, 2005; Horne et al., 2005a; Horne et al., 2005b; Shprits et al., 2006; Omura et al., 2007; Summers et al., 2007; Omura et al., 2008; Albert et al., 2009; Thorne, 2010]. One characteristic has remained invariant though; the resonance between VLF waves and relativistic electrons takes place locally, on a given flux tube, without transporting the electrons radially. This local acceleration is therefore fundamentally different from radial-diffusive acceleration in both the energization process and the source population.

However, prior to the launch of the Van Allen Probes satellites, the measurements needed to clearly distinguish between the two types of acceleration process. A radially localized peak in electron fluxes (at a given energy) can be produced by either local or radial-diffusive acceleration. It was widely recognized in the radiation belt community that it would be necessary to convert measurements of electron flux, j, to phase space density, f. The two quantities are related by the simple formula $f = j/p^2$. The challenge comes in converting flux from its natural coordinate system (position, energy, and pitch angle) to phase space density as a function of the adiabatic invariants (μ , K, L*) that define the canonical coordinate system for relativistic electron motion [Schulz, 1996; see also GEM Inner Magnetosphere and Storms Campaign Working Group report, 1999 (http://www-ssc.igpp.ucla.edu/gem/work_groups/ims_wg2.html)]. In any realistic magnetic field the conversion from $j(\vec{r}, E, \alpha)$ to $f(\mu, K, L^*)$ is both unique and time dependent for any point along a satellite's orbit. Fortunately, new global magnetic field models, combined with improvements in computational power, have made

this conversion significantly more efficient and robust. Advanced magnetic field models, in particular, are especially important, as accurate phase space density calculations are highly dependent on the accuracy of the field models [e.g., Turner and Li, 2008; Turner et al., 2012].

3.5 Phase space density gradients

Radial diffusion occurs whenever various processes produce field fluctuations on the time scale of electron drifts. At some level, these fluctuations always exist so radial diffusion is always operating in the Earth's radiation belts—either at rapid rates or slower rates. Since diffusion always moves a quantity from a region of higher density to lower, the radial gradients of phase space density (i.e., $f(L^*)$ at fixed μ and K) will be positive (increasing with radial distance) if electrons are diffusing inward from a magnetotail source population, whereas they will be negative (decreasing with radial distance) in the outer part of the belt if the electrons are accelerated locally and the magnetotail/magnetopause acts as a sink. Another advantage of analysing radial gradients of phase space density is that the adiabatic changes are 'automatically' accounted for. When phase space density is plotted as a function of L* (and L* is calculated in a realistic field model), phase space density on that drift shell does not change when the magnetic field changes. In the absence of acceleration or loss, L* (for a given μ , K) defines a surface of constant phase space density, $f(\mu, K, L^*) = const.$ Therefore the only way to unambiguously identify radial diffusion, acceleration, or loss is to look for changes in phase space density, e.g., $f(\mu, K, L^*, t)$, which are the signatures of violation of one or more adiabatic invariants.

The next couple of figures illustrate, schematically, the changes in phase space density profiles expected from radial diffusion (D_{LL} , Figure 3.9) and local acceleration (D_{EE} , Figure 3.10). Phase space density profiles are represented for three different times with the lower, middle, and upper lines respectively. If the phase space density at the source and sink do not vary with time, then increasing radial diffusion will move electrons inward, flattening the gradient at high L* where diffusion is strongest (Figure 3.9). In the inner regions (L* \approx 4–5) the phase space density increases locally but the increase is due to the radial transport of electrons. Stated another way, the phase space density is not conserved, $f(\mu, K, L^*, t) \neq const$, because 'new' electrons are added from the source region. Note, however, that regardless of how strong the radial diffusion is, the radial gradient will always be positive and monotonic from the sink (slot region) to the source (magnetotail).

VLF waves energize electrons locally through energy diffusion and produce a distinctively different change in phase space density profiles—a radially localized peak that grows from the background distribution to produce negative radial gradients at high L* (Figure 3.10). Here again the phase space density increases in the inner regions (L* \approx 4–5) but the increase is due to the local acceleration of electrons. In this case, $f(\mu, K, L^*, t) \neq const$ because acceleration (energy diffusion) does not conserve μ .

There are, however, complications to what otherwise would be a fairly straightforward measurement as illustrated in Figures 3.11 and 3.12. Firstly, the fluxes of electrons and

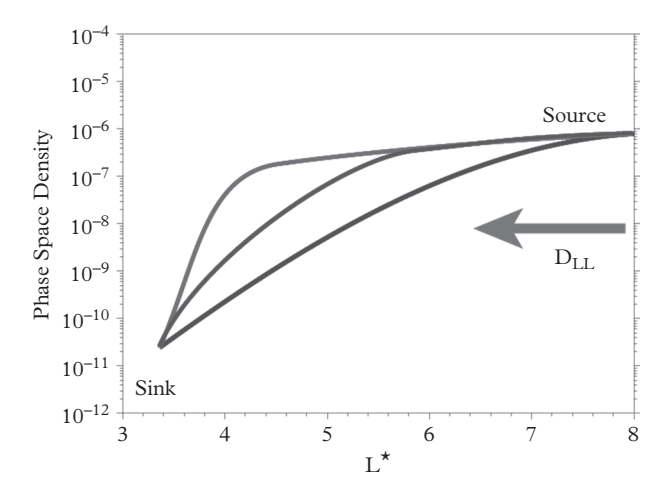


Figure 3.9 A schematic of radial diffusion from a source region (the magnetotail) to a sink region (the slot). An increase in radial diffusion will increase the transport rate and increase the phase space densities in the heart of the outer radiation belt ($L^* \approx 4-5$) [from Reeves, 2015].

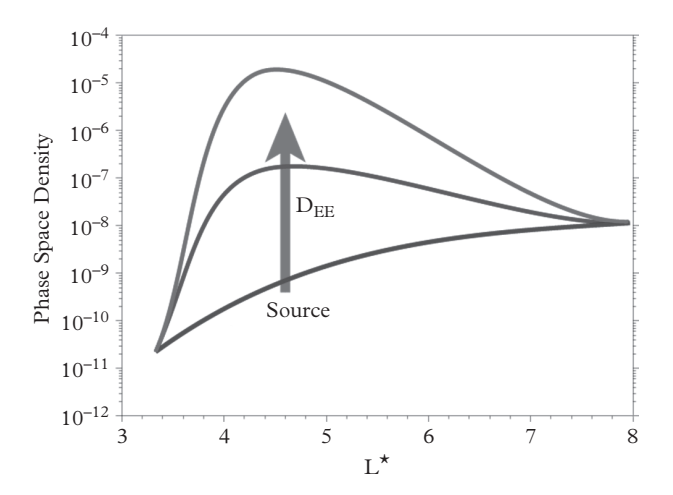


Figure 3.10 A schematic of local acceleration. Wave-particle interactions produce energy diffusion that accelerates electrons. In this case the source of the relativistic electrons is the local lower-energy electron population [from Reeves, 2015].

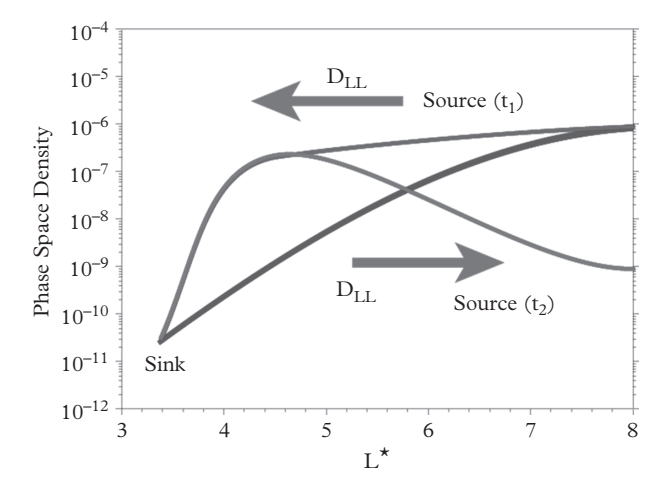


Figure 3.11 A schematic showing how peaks in phase space density can be formed by a combination of radial diffusion and a variable source at high L^* [from Reeves, 2015].

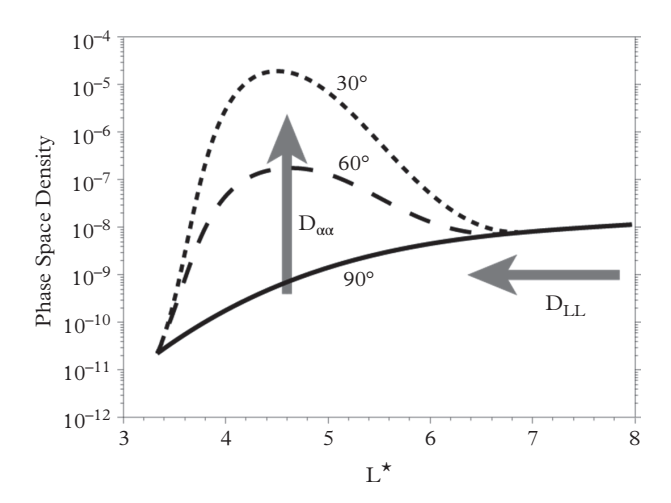


Figure 3.12 A schematic of the different radial profiles of phase space density that can be produced for different equatorial pitch angles (K values) through a combination of radial diffusion and localized pitch angle diffusion [from Reeves, 2015].

ions at the inner edge of the plasma sheet are not constant. Therefore the 'source' in Figure 3.9 can be time-variable. As illustrated in Figure 3.11, if the source at time t1 is high then radial diffusion will transport electrons earthward. If at time t2 the source is lower then diffusion will transport electrons outward. Since diffusion is faster at higher L than at lower L a phase space density peak can be produced without local acceleration. Phase space density peaks can also be produced by a combination of radial diffusion and pitch angle diffusion, without energy diffusion (Figure 3.12). This possibility leaves ambiguities in studies using off-equatorial measurements.

3.6 Studies with the Van Allen Probes: insights into the effects of wave-particle interactions and the ring current influence

NASA's Van Allen Probes mission (formerly Radiation Belt Storm Probes—RBSP) was designed, in part, to overcome the observational limitations of previous missions and differentiate clearly between radial-diffusive acceleration and local wave-particle acceleration [Kessel et al., 2012; Mauk et al., 2012]. The Van Allen Probes are a pair of satellites with a comprehensive set of particle and fields instruments in an equatorial, elliptical orbit with apogee at $\approx\!5.8~R_E$. Their orbital period is $\approx\!9$ hours but is slightly different for the two satellites. This allows for the phasing in the orbits to vary with time. At times the satellites are perfectly out of phase with apogees separated by only 4.5 hours, passing through the heart of the belts every 2–3 hours. This unprecedented temporal resolution, near-equatorial orbit, and paired satellite configuration is providing views of radiation belt dynamics that were not previously possible.

In order to resolve whether or not local acceleration by VLF waves was a viable mechanism for accelerating radiation belt electrons, Reeves et al. [2013] analysed phase space density profiles for a storm that occurred on October 8–9, 2012, early in the Van Allen Probes mission. The October 2012 storm produced a strong and rapid enhancement of the fluxes in the outer electron belt and the first opportunity to test whether or not local wave-particle interactions are a viable mechanism for relativistic electron acceleration. The 2 MeV electron fluxes at L \approx 4.2 increased by nearly three orders of magnitude in approximately 12 hours. The unique configuration of the Van Allen Probes was able to capture the rapid transformation of the belts in a way that definitively ruled out the other possibilities for producing radial peaks in phase space density during this particular storm.

Figure 3.13 shows profiles of phase space density as a function of L* for fixed values of μ and K. Reeves et al. [2013] used the TS04 [Tsyganenko and Sitnov, 2005] magnetic field model to calculate the adiabatic invariants. In Figure 3.13 each radial pass is labelled by the time at which the satellite crosses L* = 4.2. Here phase space densities are for μ = 3433 MeV/G and K = 0.11 G^{1/2} R_E (E \approx 2–6 MeV and 50° < α_e < 90° depending on the point on the orbit). Between 23:17 UT on October 8 and 03:12 UT on October 9,

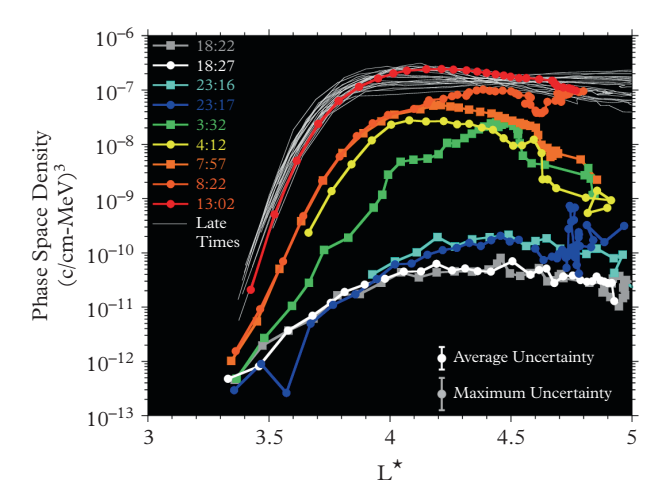


Figure 3.13 Radial profiles of phase space density measured by the two NASA Van Allen Probes satellites on October 8–9, 2012. A rapid increase in phase space density in a region centred near $L^*\approx 4.2$, a slower increase in the outer portion of the belt ($L^*>4.7$), and the resulting radial peaks in phase space density are the signatures expected for local wave-particle acceleration [from Reeves et al., 2013].

phase space densities increased by approximately two orders of magnitude at $L^* = 4.2$ and continued increasing until about 13:02 UT when the IMF turned northward.

On October 8-9, 2012, the Van Allen Probes were nearly perfectly out of phase in their orbits. This provided the fastest possible time resolution but also provided simultaneous measurements at high and low L*. During this time, RBSP-B measured a positive radial gradient at L*<4.2. At the same time, RBSP-A measured a negative radial gradient at L*>4.2, showing that the radial peak in phase space density was not an artefact of spatial-temporal aliasing. At 08:12 UT, by coincidence, the orbital dynamics were such that both spacecraft reached L* ≈ 4.2 at the same time. Although the satellites were at quite different local times, the satellites should measure the same phase space density when they are on the same L^* (a 'drift shell conjunction'). Any mismatches provide limits on uncertainties due to instrument calibration and also to uncertainties in the calculation of the invariant integrals [Morley et al., 2013]. Reeves et al. used this (and other techniques) to determine that the average and worst-case uncertainties were a factor of 1.4 and 2.0 respectively. They were also able to rule out time dependence of the plasma sheet source population (Figure 3.11) using simultaneous, multi-satellite geosynchronous measurements. These measurements pointed to local wave-particle acceleration as the only viable process and strongly suggested that acceleration by VLF chorus was the proximate cause.

Thorne et al. [2013], studying the same event, used measured VLF chorus wave amplitudes and frequency distributions to calculate the energy (momentum) and pitch angle diffusion coefficients in the heart of the acceleration region at $L^*\approx 4.2$. They applied a 2D diffusion solver to the initial pitch angle and energy distribution measured by the REPT instrument [Baker et al., 2012] and found that resonant interaction with chorus waves could fully explain the evolution of the MeV electron distribution.

Tu et al. [2014] were able to investigate the October 2012 event in even more detail using the DREAM-3D diffusion code and a remarkably complete set of observations to constrain the boundary conditions and free parameters. They were able to quantitatively illustrate the complex interplay of chorus acceleration, electron losses, and radial diffusion. A particularly important component of the simulation turned out to be the low-energy 'seed population'—a topic further investigated by Boyd et al. [2014]. Studies of relativistic electron acceleration by VLF chorus continue to produce a more-and-more detailed picture of this mechanism [Foster et al., 2014; Li et al., 2014c; Su et al., 2014a; Liu et al., 2015].

Within the plasmasphere, VLF waves are primarily observed in the form of broadband, incoherent hiss. While chorus and hiss are both whistler-mode waves, hiss is relatively inefficient at producing acceleration and primarily produces losses through pitch angle scattering. Common understanding would suggest that ring current electrons only penetrate the plasmasphere in the plume regions but Van Allen observations have shown that ring current electrons can sometimes (but rarely) be directly injected into the plasmasphere where they can provide a source of free energy for the generation of hiss [Chen et al., 2014; Li et al., 2014a; Li et al., 2014b; Ni et al., 2014]. Other studies have shown that plasmaspheric hiss can also result from whistler-mode chorus waves that are generated at higher L-shells, outside the plasmasphere, and subsequently refracted at high latitudes into the plasmasphere [e.g., Bortnik et al., 2007; 2009].

As the Van Allen Probes are equipped with a complete complement of fields and waves instruments [Kletzing et al., 2013; Wygant et al., 2014], more comprehensive investigations of ring current associated fields and waves that are important for radiation belt dynamics have become possible. One example are storm-time mechanisms for the acceleration of the initial seed population of 100s keV electrons. Mozer et al. [2014] and Malaspina et al. [2014] found evidence of local acceleration from non-linear electric field structures associated with substorm injections and the transport of electrons and ions into the ring current.

Much attention has been focused on the production of whistler waves by unstable plasma distributions in storm-time substorm injections and the electron component of the ring current. Furthermore, there are other important radiation belt processes associated with the ion component of the ring current. The Van Allen Probes measurements have been able to confirm and add considerable detail to the importance of magnetopause losses caused, not only by earthward motion of the magnetopause, but also by the outward, adiabatic transport of radiation belt electrons [Shprits et al., 2013; Hudson et al., 2014; Turner et al., 2014a; Turner et al., 2014b]. Unstable ring current ion distributions also produce radiation belt-effective waves and are being studied

in unprecedented detail. Electromagnetic ion cyclotron (EMIC) waves, excited by the injection of ring current ions, can cause rapid precipitation loss of relativistic electrons on timescales of a few hours [e.g., Bortnik et al., 2006], but may only act on the most energetic part of the radiation belts (although the precise energy range is hotly debated). New observations from the Van Allen Probes shed light not only on the effect of EMIC waves but also on how they are generated and what their characteristics are [Allen et al., 2013; Shprits et al., 2013; Usanova et al., 2014; Zhang et al., 2014].

Magnetosonic waves [Ma et al., 2014; Zhao et al., 2014; Zhou et al., 2014] are another candidate for radiation belt electron acceleration—although it is not clear whether they can efficiently accelerate relativistic electrons. Last but not least, radial diffusion operates to redistribute and accelerate (or decelerate) electrons [Baker et al., 2014; Li et al., 2014d] producing the remarkable spatial coherence observed in the radiation belts. The Van Allen Probes have also provided the most detailed observational evidence to date for drift resonant interactions between radiation belt electrons and ULF waves [Claudepierre et al., 2013; Dai et al., 2013; Mann et al., 2013], which may be driven by low-frequency mirror and drift instabilities of ring current ion populations [Ozeke and Mann, 2008; Ge et al., 2011].

3.7 Summary

We have presented an overview of the complex influence of geospace magnetic storms on the dynamics of the Van Allen radiation belts—in particular the outer (electron) belt. Although the basic build-up and decay of the storm-time ring current and of the radiation belts are fundamentally similar, the acceleration of energetic 'seed' electrons to relativistic energies and their loss through atmospheric precipitation are rather distinct. The comprehensive suite of particles and fields instruments on-board the Van Allen Probes, in combination with the advances in computational power and magnetic field modelling, allow the efficient conversion of fluxes to phase space densities and the extraction of wave characteristics. Thus, the impacts of storm-associated fields and waves on the acceleration and loss of radiation belt electrons can be identified and assessed, making now-casting and forecasting of radiation belt content and intensity a realistic goal for the not-too-distant future.

Acknowledgments

The work leading to this paper was supported by RBSP-ECT funding under NASA's Prime contract no. NAS5- 01072, by the Dynamic Radiation Environment Assimilation Model (DREAM) project at Los Alamos National Laboratory, and by the European Union's Seventh Framework Programme (FP7-SPACE-2011-1) grant agreement no. 284520 for the 'Monitoring, Analyzing and Assessing Radiation Belt Energization and Loss' (MAARBLE) collaborative research project.

.....

REFERENCES

- Albert, J. M., and S. L. Young (2005), Multidimensional quasi-linear diffusion of radiation belt electrons, *Geophys. Res. Lett.*, 32, L14110, doi:10.1029/2005GL023191.
- Albert, J. M., et al. (2009), Three-dimensional diffusion simulation of outer radiation belt electrons during the 9 October 1990 magnetic storm, J. Geophys. Res., 114, A09214, doi:10.1029/2009JA014336.
- Allen, R. C., et al. (2013), Multiple bidirectional EMIC waves observed by Cluster at middle magnetic latitudes in the dayside magnetosphere, *J. Geophys. Res.: Space Phys.*, 118, 10, doi:10.1002/Jgra.50600.
- Baker, D. N., et al. (1989), Relativistic electrons near geostationary orbit: Evidence for internal magnetospheric acceleration, *Geophys. Res. Lett.*, **16**, 6, doi:10.1029/GL016i006p00559.
- Baker, D. N., et al. (1998), Coronal mass ejections, magnetic clouds, and relativistic magnetospheric electron events: ISTP, J. Geophys. Res.: Space Phys., 103, A8, doi: 10.1029/97ja03329.
- Baker, D. N., et al. (1999), Equinoctial and solstitial averages of magnetospheric relativistic electrons: A strong semiannual modulation, *Geophys. Res. Lett.*, **26**, 20, doi:10.1029/1999gl003638.
- Baker, D. N., et al. (2012), The relativistic electron-proton telescope (REPT) instrument on board the Radiation Belt Storm Probes (RBSP) spacecraft: Characterization of Earth's radiation belt high-energy particle populations, *Space Sci. Rev.*, doi:10.1007/s11214-012-9950-9.
- Baker, D. N., et al. (2013), A long-lived relativistic electron storage ring embedded in Earth's outer Van Allen belt, *Science*, 340, 6129, doi:10.1126/science.1233518.
- Baker, D. N., et al. (2014), Gradual diffusion and punctuated phase space density enhancements of highly relativistic electrons: Van Allen Probes observations, *Geophys. Res. Lett.*, 41, 5, doi:10.1002/2013gl058942.
- Blake, J. B., et al. (1997), Correlation of changes in the outer-zone relativistic electron population with upstream solar wind and magnetic field measurements, *Geophys. Res. Lett.*, 24, 8, doi:10.1029/97GL00859.
- Borovsky, J. E., and M. H. Denton (2006), Differences between CME-driven storms and CIR-driven storms, *J. Geophys. Res.*, 111, A07S08, doi:10.1029/2005JA011447.
- Borovsky, J. E., and M. H. Denton (2011), A survey of the anisotropy of the outer electron radiation belt during high-speed-stream-driven storms, J. Geophys. Res.-Space, 116, doi:10.1029/2010ja016151.
- Bortnik, J., R. M. Thorne, T. P. O'Brien, J. C. Green, R. J. Strangeway, Y. Y. Shprits, and D. N. Baker (2006), Observation of two distinct, rapid loss mechanisms during the 20 November 2003 radiation belt dropout event, J. Geophys. Res., 111, A12216, doi:10.1029/2006JA01 1802.
- Bortnik, J., R. M. Thorne, N. P. Meredith, and O. Santolik (2007), Ray tracing of penetrating chorus and its implications for the radiation belts, *Geophys. Res. Lett.*, 34, L15109, doi:10.1029/2007GL030040.
- Bortnik, J., W. Li, R. M. Thorne, V. Angelopoulos, C. M. Cully, J. W. Bonnell, O. LeContel, and A. Roux (2009), An observation linking the origin of plasmaspheric hiss to discrete chorus emissions, *Science*, 324, 775–778.
- Boyd, A. J., et al. (2014), Quantifying the radiation belt seed population in the 17 March 2013 electron acceleration event, *Geophys. Res. Lett.*, 41, 7, doi: 10.1002/2014gl059626.
- Chapman, S., and V. C. A. Ferraro (1930), A new theory of magnetic storms, *Nature*, 126, 129–130.

- Chapman, S., and V. C. A. Ferraro (1931), A new theory of magnetic storms, I. The initial phase, *Terrest. Magn. Atmosph. Elec.*, **36**, 77–97, 171–186.
- Chen, L., et al. (2014), Generation of unusually low frequency plasmaspheric hiss, *Geophys. Res. Lett.*, 41, 16, doi:10.1002/2014gl060628.
- Claudepierre, S. G., et al. (2013), Van Allen Probes observation of localized drift resonance between poloidal mode ultra-low frequency waves and 60 kev electrons, *Geophys. Res. Lett.*, 40, 17, doi:10.1002/Grl.50901.
- Clilverd, M. A., et al. (2010), Energetic outer radiation belt electron precipitation during recurrent solar activity, J. Geophys. Res., 115, A8, doi:10.1029/2009ja015204.
- Daglis, I. A. (1997), The role of magnetosphere-ionosphere coupling in magnetic storm dynamics, in *Magnetic Storms*, *Geophys. Monogr. Ser.*, vol. 98, edited by B. T. Tsurutani et al., pp. 107–116, AGU, Washington, D. C.
- Daglis, I. A., E. T. Sarris, and B. Wilken (1993), AMPTE/CCE CHEM observations of the ion population at geosynchronous altitudes, Ann. Geophys., 11, 685–696.
- Daglis, I. A., R. M. Thorne, W. Baumjohann, and S. Orsini (1999), The terrestrial ring current: Origin, formation, evolution and decay, Rev. Geophys., 37(4), 407–438, doi:10.1029/1999RG900009.
- Daglis, I.A. (2006), Ring current dynamics, *Space Sci. Rev.*, **124**, 183–202, doi: 10.1007/s11214-006-9104-z.
- Dai, L., et al. (2013), Excitation of poloidal standing alfvén waves through drift resonance wave-particle interaction, *Geophys. Res. Lett.*, **40**, 16, doi:10.1002/grl.50800.
- Denton, M. H., and J. E. Borovsky (2012), Magnetosphere response to high-speed solar wind streams: A comparison of weak and strong driving and the importance of extended periods of fast solar wind, *J. Geophys. Res.*, 117, doi:10.1029/2011ja017124.
- Dungey, J. W. (1963), Loss of van allen electrons due to whistlers, *Planet. Space Sci.*, 11, 6, doi:10.1016/0032-0633(63)90166-1.
- Fälthammar, C. G. (1965), Effects of time-dependent electric fields on geomagnetically trapped radiation, J. Geophys. Res., 70, 11, doi:10.1029/Jz070i011p02503.
- Fennell, J. F., et al. (2015), Van Allen Probes show that the inner radiation zone contains no MeV electrons: ECT/MagEIS data, *Geophys. Res. Lett.*, 42, 5, doi:10.1002/2014gl062874.
- Foster, J. C., et al. (2014), Prompt energization of relativistic and highly relativistic electrons during a substorm interval: Van Allen Probes observations, *Geophys. Res. Lett.*, 41, 1, doi:10.1002/2013gl058438.
- Frank, L. A. (1967), On the extraterrestrial ring current during geomagnetic storms, *J. Geophys. Res.*, 72, 3753–3767.
- Friedel, R. H. W., et al. (1999), A multi-spacecraft synthesis of relativistic electrons in the inner magnetosphere using LANL, GOES, GPS, SAMPEX, HEO and Polar, *Radiat. Meas.*, **30**, 5, doi:10.1016/S1350-4487(99)00230-9.
- Friedel, R.H.W., et al. (2002), Relativistic electron dynamics in the inner magnetosphere a review, *J. Atmos. Sol.-Terr. Phy.*, **64**, 2, doi:Pii S1364-6826(01)00088-8.
- Ge, Y.S., J.P. McFadden, J. Raeder, V. Angelopoulos, D. Larson, and O.D. Constantinescu (2011), Case studies of mirror-mode structures observed by THEMIS in the near-Earth tail during substorms, J. Geophys. Res., 116, A01209, doi:10.1029/2010JA015546.
- Goodrich, C. C., et al. (1998), An overview of the impact of the January 10–11 1997 magnetic cloud on the magnetosphere via global MHD simulation, *J. Geophys. Res.*, 25, 14, doi:10.1029/98GL01159.
- Hamilton, D. C., G. Gloeckler, F. M. Ipavich, W. Stüdemann, B. Wilken, and G. Kremser (1988), Ring current development during the great geomagnetic storm of February 1986, J. Geophys. Res., 93, 14,343–14,355.

- Hietala, H., et al. (2014), Depleting effects of ICME-driven sheath regions on the outer electron radiation belt, *Geophys. Res. Lett.*, 41, 7, doi:10.1002/2014gl059551.
- Horne, R. B., and R. M. Thorne (1998), Potential waves for relativistic electron scattering and stochastic acceleration during magnetic storms, *Geophys. Res. Lett.*, 25, 15, doi:10.1029/98GL01002.
- Horne, R. B., et al. (2000), Proton and electron heating by radially propagating fast magnetosonic waves, J. Geophys. Res., 105, 27597–27610.
- Horne, R. B. (2002), The contribution of wave particle interactions to electron loss and acceleration in the earth's radiation belts during geomagnetic storms, in *Review of Radio Science* 1999–2002, edited by W. R. Stone, chapter 33, pp. 801–828, Wiley, New York City.
- Horne, R. B., and R. M. Thorne (2003), Relativistic electron acceleration and precipitation during resonant interactions with whistler-mode chorus, *Geophys. Res. Lett.*, 30, 10, doi:10.1029/2003GL016973.
- Horne, R. B., et al. (2005a), Timescale for radiation belt electron acceleration by whistler mode chorus waves, *J. Geophys. Res.: Space.*, **110**, A3, doi:10.1029/2004ja010811.
- Horne, R. B., et al. (2005b), Wave acceleration of electrons in the van allen radiation belts, *Nature*, 437, 8, doi:doi:10.1038/nature03930.
- Hudson, M. K., et al. (2000), Increase in relativistic electron flux in the inner magnetosphere: Ulf wave mode structure, *Adv. Sp. Res.*, 25, 12, doi:10.1016/S0273-1177(99)00518-9.
- Hudson, M. K., et al. (2001), Radiation belt electron acceleration by ULF wave drift resonance: Simulation of 1997 and 1998 storms in *Space Weather*, Geophys. Monogr. Ser., vol. 125, edited by P. Song et al., pp. 289–296, AGU, Washington, D. C.
- Hudson, M. K., et al. (2014), Simulated magnetopause losses and Van Allen Probe flux dropouts, Geophys. Res. Lett., doi:10.1002/2014gl059222.
- Jordanova, V. K., et al. (1998), Effect of wave-particle interactions on ring current evolution for January 10 11, 1997: Initial results, Geophys. Res. Lett., 25(15), 2971–2974, 10.1029/98GL00649.
- Jordanova, V. K., et al. (1999), Ring current activity during the early Bz<0 phase of the January 1997 magnetic cloud, J. Geophys. Res., 104(A11), 24895–24914, doi: 10.1029/1999JA900339.
- Kamide, Y., J.-H. Shue, X. Li, G. Lu, M. Brittnacher, G. Parks, and G. D. Reeves (1998), Internally and externally triggered substorms: A case study of the January 10, 1997 events, in *Proceedings of the 4th International Conference on Substorms*, edited by S. Kokubun and Y. Kamide, pp. 305–309, Kluwer Academic Publishers.
- Kellogg, P. J. (1959), Possible explanation of the radiation observed by Van Allen at high altitude in satellites, Il Nuovo Cimento, 11, pp. 48–66.
- Kennel, C. F., and H. E. Petschek (1966), Limit on stably trapped particle fluxes, J. Geophys. Res., 71, 1, doi:10.1029/JZ071i001p00001.
- Kessel, R. L., et al. (2012), The Radiation Belt Storm Probes (RBSP) and space weather, Space Sci. Rev., doi:10.1007/s11214-012-9953-6.
- Kilpua, E. K. J., H. Hietala, D. L. Turner, H. E. J. Koskinen, T. I. Pulkkinen, J. V. Rodriguez, G. D. Reeves, S. G. Claudepierre, and H. E. Spence (2015), Unraveling the drivers of the storm time radiation belt response, *Geophys. Res. Lett.*, 42, doi:10.1002/2015GL063542.
- Kim, H. J., and A. A. Chan (1997), Fully adiabatic changes in storm-time relativistic electron fluxes, *J. Geophys. Res.: Space*, **102**, A10, doi:10.1029/97ja01814.
- Kletzing, C. A., et al. (2013), The electric and magnetic field instrument suite and integrated science (EMFISIS) on RBSP, *Space Sci. Rev.*, doi:10.1007/s11214-013-9993-6.
- Li, W., et al. (2014a), Evidence of stronger pitch angle scattering loss caused by oblique whistler-mode waves as compared with quasi-parallel waves, *Geophys. Res. Lett.*, doi:10.1002/2014gl061260.

- Li, W., et al. (2014b), Quantifying hiss-driven energetic electron precipitation: A detailed conjunction event analysis, *Geophys. Res. Lett.*, **41**, 4, doi:10.1002/2013gl059132.
- Li, W., et al. (2014c), Radiation belt electron acceleration by chorus waves during the 17 March 2013 storm, J. Geophys. Res., 119, 6, doi: 10.1002/2014ja019945.
- Li, X. L., et al. (1997), Multisatellite observations of the outer zone electron variation during the November 3–4, 1993, magnetic storm, *J. Geophys. Res.*, **102**, A7, doi: 10.1029/97ja01101.
- Li, Z., et al. (2014d), Radial diffusion comparing a THEMIS statistical model with geosynchronous measurements as input, J. Geophys. Res.: Space Phys., doi:10.1002/2013ja019320.
- Liu, S., et al. (2015), Van Allen Probes observations linking radiation belt electrons to chorus waves during 2014 multiple storms, J. Geophys. Res.: Space Phys., 120, 938–948, doi:10.1002/2014JA020781.
- Lyons, L. R., and R. M. Thorne (1973), Equilibrium structure of radiation belt electrons, *J. Geophys. Res.*, 78, 13, doi:10.1029/Ja078i013p02142.
- Lyons, L. R., et al. (2000), Auroral disturbances during the January 10, 1997 magnetic storm, *Geophys. Res. Lett.*, 27, 20, doi:10.1029/1999gl000014.
- Ma, Q., et al. (2014), The trapping of equatorial magnetosonic waves in the earth's outer plasmasphere, *Geophys. Res. Lett.*, 41, 18, doi:10.1002/2014gl061414.
- Malaspina, D. M., et al. (2014), Nonlinear electric field structures in the inner magnetosphere, *Geophys. Res. Lett.*, **41**, 16, doi:10.1002/2014gl061109.
- Mann, I. R., et al. (2013), Discovery of the action of a geophysical synchrotron in the earth's van allen radiation belts, *Nat. Commun.*, 4, Doi:10.1038/Ncomms3795.
- Mauk, B. H., et al. (2012), Science objectives and rationale for the Radiation Belt Storm Probes mission, *Space Sci. Rev.*, doi:10.1007/s11214-012-9908-y.
- Millan, R. M., and R. M. Thorne (2007), Review of radiation belt relativistic electron loss, *J. Atmos. Sol.-Terr. Phys.*, **69**.
- Miyoshi, Y. S., et al. (2004), Solar cycle variations of the electron radiation belts: Observations and radial diffusion simulation, *Space Weather*, 2, S10S02, doi:10.1029/2004SW000070.
- Miyoshi, Y., and R. Kataoka (2005), Ring current ions and radiation belt electrons during geomagnetic storms driven by coronal mass ejections and corotating interaction regions, *Geophys. Res. Lett.*, **32**, 21, doi:10.1029/2005gl024590.
- Morley, S. K., et al. (2013), Phase space density matching of relativistic electrons using the Van Allen Probes: REPT results, *Geophys. Res. Lett.*, **40**, 18, doi:10.1002/Grl.50909.
- Mozer, F. S., et al. (2014), Direct observation of radiation-belt electron acceleration from electron-volt energies to megavolts by nonlinear whistlers, *Phys. Rev. Lett.*, **113**, 3, doi:10.1103/PhysRevLett.113.035001.
- Ni, B. B., et al. (2014), Resonant scattering of energetic electrons by unusual low-frequency hiss, *Geophys. Res. Lett.*, **41**, 6, doi:10.1002/2014gl059389.
- Nishida, A. (1976), Outward diffusion of energetic particles from the Jovian radiation belt, *J. Geophys. Res.*, **81**, 10, doi:10.1029/JA081i010p01771.
- Northrop, T., and E. Teller (1960), Stability of the adiabatic motion of charged particles in the earth's field, *Phys. Rev.*, 117, 1, doi:10.1103/PhysRev.117.215.
- O'Brien, T. P., et al. (2003), Energization of relativistic electrons in the presence of ULF power and MeV microbursts: Evidence for dual ULF and VLF acceleration, J. Geophys. Res., 108 (A8), 1329, doi:10.1029/2002JA009784.
- Omura, Y., et al. (2007), Relativistic turning acceleration of resonant electrons by coherent whistler mode waves in a dipole magnetic field, J. Geophys. Res., 112, A06236, doi:10.1029/2006JA012243.

- Omura, Y., et al. (2008), Theory and simulation of the generation of whistler-mode chorus, J. Geophys. Res., 113, A04223, doi:10.1029/2007JA012622.
- Onsager, T. G., et al. (2002), Radiation belt electron flux dropouts: Local time, radial, and particle-energy dependence, J. Geophys. Res., 107, A11, doi: 10.1029/2001ja000187.
- Ozeke, L. G., and I. R. Mann (2008), Energization of radiation belt electrons by ring current ion driven ULF waves, J. Geophys. Res., 113, A02201, doi:10.1029/2007JA012468.
- Paulikas, G. A., and J. B. Blake (1979), Effects of the solar wind on magnetospheric dynamics: Energetic electrons at the synchronous orbit, in *Quantitative Modeling of Magnetospheric Processes*, edited by W.P. Olson, pp. 180–202.
- Reeves, G. D. (1998), Relativistic electrons and magnetic storms: 1992–1995, *Geophys. Res. Lett.*, 25, 11, doi:10.1029/98gl01398.
- Reeves, G. D., et al. (1998a), The global response of relativistic radiation belt electrons to the January 1997 magnetic cloud, *Geophys. Res. Lett.*, 25, 17, doi:10.1029/98gl02509.
- Reeves, G. D., et al. (1998b), The relativistic electron response at geosynchronous orbit during the January 1997 magnetic storm, *J. Geophys. Res.*, 103, A8, doi:10.1029/97JA03236.
- Reeves, G. D., et al. (2003), Acceleration and loss of relativistic electrons during geomagnetic storms, *Geophys. Res. Lett.*, **30**, 10, doi:10.1029/2002gl016513.
- Reeves, G. D., et al. (2012), Dynamic radiation environment assimilation model: DREAM, *Space Weather*, **10**, doi:10.1029/2011sw000729.
- Reeves, G. D., et al. (2013), Electron acceleration in the heart of the van allen radiation belts, *Science*, 341, 6149, doi:10.1126/science.1237743.
- Reeves, G. D. (2015), Radiation belt electron acceleration and role of magnetotail, in *Magnetotails in the Solar System*, edited by A. Keiling, C. M. Jackman, and P. A. Delamere, John Wiley & Sons, Inc., doi: 10.1002/9781118842324.
- Reeves, G. D., et al. (2016), Energy-dependent dynamics of keV to MeV electrons in the inner zone, outer zone, and slot regions, *J. Geophys. Res.: Space Phys.*, 121, 1, doi:10.1002/2015ja021569.
- Roederer, J. G. (1970), Dynamics of Geomagnetically Trapped Radiation, Springer-Verlag, New York.
- Russell, C. T., and R. L. McPherron (1973), Semiannual variation of geomagnetic activity, J. Geophys. Res., 78, 1, doi:10.1029/JA078i001p00092.
- Schiller, Q., et al. (2014), A nonstorm-time enhancement of relativistic electrons in the outer radiation belt, *Geophys. Res. Lett.*, 41, 1, doi:10.1002/2013gl058485.
- Schulz, M., and L. J. Lanzerotti (1974), Particle Diffusion in the Radiation Belts, Springer-Verlag, New York.
- Schulz, M. (1996), Canonical coordinates for radiation belt modeling, in *Radiation Belt Models and Standards*, edited by J. F. Lemaire et al., pp. 153–161, American Geophysical Union, Washington DC.
- Selesnick, R. S., et al. (2007), A theoretical model of the inner proton radiation belt, *Space Weather*, 5, S04003, doi:10.1029/2006SW000275.
- Shprits, Y. Y., et al. (2006), Bounce-averaged diffusion coefficients for field-aligned chorus waves, *J. Geophys. Res.*, 111, A10225, doi:10.1029/2006JA011725.
- Shprits, Y. Y., et al. (2013), Unusual stable trapping of the ultrarelativistic electrons in the van allen radiation belts, *Nat. Phys.*, **9**, 11, doi:10.1038/Nphys2760.
- Singer, S. F. (1958), Trapped albedo theory of the radiation belt, *Phys. Rev. Lett.*, 1, 5, doi:10.1103/Physrevlett.1.181.
- Su, Z., et al. (2014a), Quantifying the relative contributions of substorm injection and chorus waves to the rapid outward extension of electron radiation belt, J. Geophys. Res., submitted, doi:10.1002/2014JA020709.

- Su, Z. P., et al. (2014b), Nonstorm-time dynamics of electron radiation belts observed by the Van Allen Probes, *Geophys. Res. Lett.*, 41, 2, doi:10.1002/2013gl058912.
- Summers, D., et al. (1998), Relativistic theory of wave-particle resonant diffusion with application to electron acceleration in the magnetosphere, J. Geophys. Res., 103, A9, doi:10.1029/98JA01740.
- Summers, D., and C. Ma (2000), A model for generating relativistic electrons in the earth's inner magnetosphere based on gyroresonant wave-particle interactions, J. Geophys. Res. 105.
- Summers, D., et al. (2002), Model of the energization of outer-zone electrons by whistler-mode chorus during the October 9, 1990, geomagnetic storm, *Geophys. Res. Lett.*, 29, 24, doi:10.1029/2002gl016039.
- Summers, D., et al. (2004), Competition between acceleration and loss mechanisms of relativistic electrons during geomagnetic storms, *J. Geophys. Res.*, **109**, A04221, doi:10.1029/2004JA010437.
- Summers, D., et al. (2007), Timescales for radiation belt electron acceleration and loss due to resonant wave-particle interactions: 1. Theory, J. Geophys. Res., 112, A04206, doi:10.1029/2006JA011801.
- Thorne, R. M. (2010), Radiation belt dynamics: The importance of wave-particle interactions, *Geophys. Res. Lett.*, 37, doi:10.1029/2010gl044990.
- Thorne, R. M., et al. (2013), Rapid local acceleration of relativistic radiation belt electrons by magnetospheric chorus, *Nature*, 504, 7480, doi:10.1038/nature12889.
- Tsyganenko, N. A., and M. I. Sitnov (2005), Modeling the dynamics of the inner magnetosphere during strong geomagnetic storms, J. Geophys. Res., 110, doi:10.1029/2004JA010798.
- Tu, W. C., et al. (2014), Event-specific chorus wave and electron seed population models in DREAM3D using the Van Allen Probes, *Geophys. Res. Lett.*, 41, 5, doi:10.1002/2013gl058819.
- Turner, D.L., and X. Li (2008), Radial gradients of phase space density of the outer radiation belt electrons prior to sudden solar wind pressure enhancements, *Geophys. Res. Lett.*, **35**, L18101, doi:10.1029/2008GL034866.
- Turner, D. L., V. Angelopoulos, Y. Shprits, A. Kellerman, P. Cruce, and D. Larson (2012), Radial distributions of equatorial phase space density for outer radiation belt electrons, *Geophys. Res. Lett.*, 39, L09101, doi:10.1029/2012GL051722.
- Turner, D. L., et al. (2014a), Competing source and loss mechanisms due to wave-particle interactions in Earth's outer radiation belt during the 30 September to 3 October 2012 geomagnetic storm, J. Geophys. Res.: Space Phys., 119, 3, doi:10.1002/2014ja019770.
- Turner, D. L., et al. (2014b), On the cause and extent of outer radiation belt losses during the 30 September 2012 dropout event, J. Geophys. Res.: Space Phys., 119, 3, doi:10.1002/2013ja019446.
- Tverskaya, L. V. (1986), On the boundary of electron injection into the magnetosphere, *Geomagn. Aeron.*, **26**, 5.
- Tverskaya, L. V., et al. (2003), Predicting the L-position of the storm-injected relativistic electron belt, *Adv. Sp. Res.*, **31**(4).
- Usanova, M. E., et al. (2014), Effect of EMIC waves on relativistic and ultrarelativistic electron populations: Ground-based and Van Allen Probes observations, *Geophys. Res. Lett.*, 41, 5, doi:10.1002/2013gl059024.
- Van Allen, J. A., et al. (1958), Observation of high intensity radiation by satellites 1958 Alpha and Gamma, *Jet Propulsion*, 28, 588–592.
- Van Allen, J. A. (1959), The geomagnetically trapped corpuscular radiation, J. Geophys. Res., 64, 1683–1689.

- Vernov, S. N., et al. (1959), Possible mechanism of production of terrestrial corpuscular radiation under the action of cosmic rays, *Sov. Phys.*, *Dokl.*, 4, 154.
- Walt, M. (1996), Source and loss processes for radiation belt particles, in *Radiation Belt Models and Standards*, edited by J. F. Lemaire et al., pp. 1–15, American Geophysical Union, Washington DC.
- Williams, D. J. (1981), Ring current composition and sources: An update, *Planet. Space Sci.*, 29, 1195-1203.
- Winckler, J. R., et al. (1962), A study of the precipitation of energetic electrons from the geomagnetic field during magnetic storms, J. Geophys. Res., 67, 10, doi:10.1029/JZ067i010p03717.
- Wygant, J. R., et al. (2014), The electric field and waves instruments on the Radiation Belt Storm Probes mission, in *The Van Allen Probes Mission*, edited by N. Fox and J. Burch, pp. 183–220, Springer US.
- Xiao-Fang, Z., et al. (2013), Effect of interplanetary disturbances and geomagnetic activities on relativistic electrons at geosynchronous orbit, *Chin. J. Geophys.*, **56**, 5, doi:10.1002/cjg2.20051.
- Zhang, J. C., et al. (2014), Excitation of EMIC waves detected by the Van Allen Probes on 28 April 2013, *Geophys. Res. Lett.*, 41, 12, doi:10.1002/2014gl060621.
- Zhao, H., et al. (2014), Peculiar pitch angle distribution of relativistic electrons in the inner radiation belt and slot region, *Geophys. Res. Lett.*, **41**, 7, doi:10.1002/2014gl059725.
- Zhou, Q., et al. (2014), Excitation of nightside magnetosonic waves observed by Van Allen Probes, *J. Geophys. Res. Space Phys.*, **119**, 9125–9133, doi:10.1002/2014JA020481.